

Pix2Vex: Image-to-Geometry Reconstruction using a Smooth Differentiable Renderer

Felix Petersen
University of Konstanz
felix.petersen@uni.kn

Amit H. Bermano
Tel Aviv University
amberman@tauex.tau.ac.il

Oliver Deussen
University of Konstanz
oliver.deussen@uni.kn

Daniel Cohen-Or
Tel Aviv University
dcor@tau.ac.il

Abstract

We present a novel approach to 3D object reconstruction from its 2D projections. Our unique, GAN-inspired system employs a novel C^∞ smooth differentiable renderer. Unlike the state-of-the-art, our renderer does not display any discontinuities at occlusions and dis-occlusions, facilitating training without 3D supervision and only minimal 2D supervision. Through domain adaptation and a novel training scheme our network, the Reconstructive Adversarial Network (RAN), is able to train on different types of images. In contrast, previous work can only train on images of a similar appearance to those rendered by a differentiable renderer. We validate our reconstruction method through three shape classes from ShapeNet, and demonstrate that our method is robust to perturbations in view directions, different lighting conditions, and levels of texture details.

1. Introduction

Reconstructing a 3D model from arbitrary images has been considered one of the holy grails of computer vision since the inception of the field. This ambitious task encapsulates many challenges, including separation of texture and shading effects, lighting estimation, and inference of occluded parts. Hence, different variants of the problem, which take advantage of different assumptions, have been tackled over the years, employing a myriad of approaches.

Perhaps the most interesting and promising approaches are those utilizing learning-based methods [1]–[18]. These can potentially exploit previously seen examples to overcome missing information such as partial visibility, unknown lighting conditions, and others. To date, most of these methods either rely on extensive manual annotation of shape [1]–[6] or key-point correspondences between images [16]–[18]. Other, less supervised methods [7]–[15] are typically restricted to settings of controlled materials, colors, lighting, and/or precise annotation of object orientation.

In this paper, we extend the interesting approach of validating a predicted reconstruction using a renderer, thus closing the image-to-geometry (*pix2vex*) and geometry-to-image (renderer) training loop. In our setting, we feed the system with grayscale images of an object from one or more directions (usually four, see Section 6), and predict its corresponding 3D geometry. In contrast to popular approaches, we provide a rough estimate of the angular difference between the aforementioned images and leave all other parameters to be deduced by the system. This means that our method does not require lighting and texture information, nor explicit 3D supervision.

This setting poses a threefold challenge. In the following, we specify these challenges, and our respective proposed solutions, which constitute the main contributions of this paper:

First, the success of such an approach depends greatly on the ability to generate meaningful gradients throughout the validation process. State-of-the-art differentiable renderers (*DRs*), however, besides being bounded by complexity and output quality, are only locally differentiable with respect to the geometry. The differentiability (or smoothness) breaks during some occlusion and dis-occlusion cases (see Section 3 for details). Hence, we present a novel C^∞ **smooth differentiable renderer**, *SR*, based on soft blending schemes of nearby triangles. This unique property is the backbone of our approach, enabling learning with minimal supervision.

Secondly, we present the image-to-geometry neural network, **pix2vex**, that is trained to predict the 3D coordinates of a given mesh topology. The network seeks to find vertex positions that produce matching renderings to the input images, while maintaining shape smoothness, with minimal supervision. A direct solution would use an auto-encoder-like network, as proposed by Che *et al.* [7]. This approach, however, restricts the network training to images that have a similar appearance to the output of the employed forward renderer (see Figure 2a). In order to extend the space of images that can be used for training, we present the following insight.

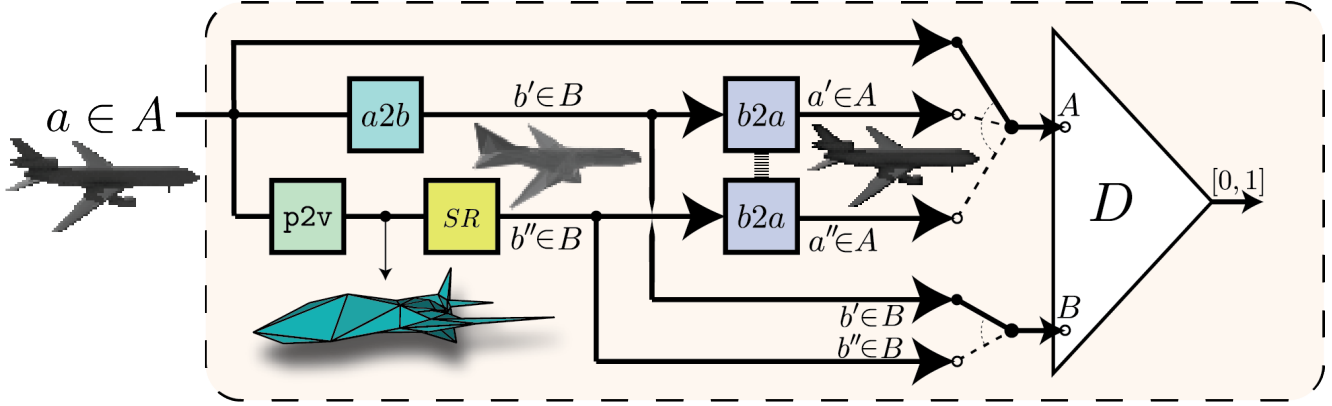


Figure 1: RAN System overview. Our image-to-geometry reconstructor ($p2v$) receives a set of images from the input domain A (e.g., grayscale images rendered by an off-the-shelf renderer) and predicts vertex positions that match. The reconstruction is validated through our novel C^∞ smooth renderer (SR). The latter produces images in a different domain, B , which are translated back to the input domain A for training purposes ($b2a$). Unlike in traditional DR -based GAN systems, the purpose of our discriminator D is to indicate whether the two inputs match in content. The whole network is trained via five different data paths, including two which require another image domain translator, $a2b$, in a novel training scheme.

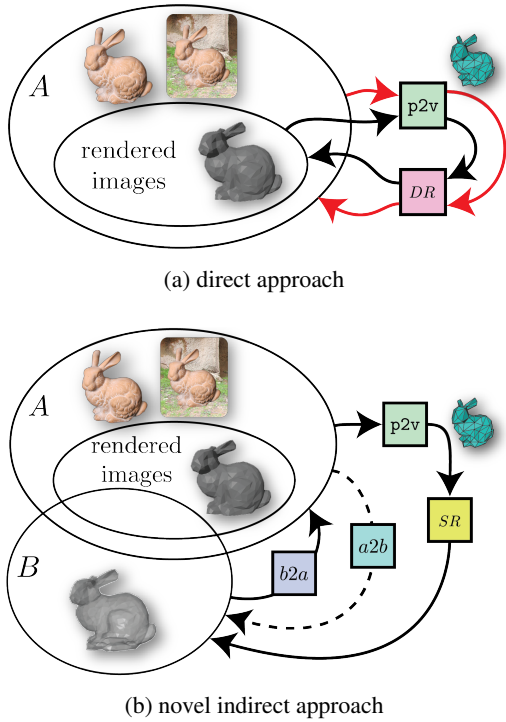


Figure 2: Traditional reconstruction approaches employing Differentiable Renderers (DR s) rely on differentially rendered images alone ((a), black path), and would fail when used with generally rendered images ((a), red path). We propose a novel *indirect* approach, in which domain translation components help in closing the training loop (b).

Due to their differential nature, DR s (and SR s) produces images which are somewhat different compared to traditional renderers. To bridge this gap, we employ an image-to-image translator, $b2a$, that converts images from our SR 's output domain, B , to images in the input one, A , and thereby closes the training loop, as depicted in Fig. 2b. Furthermore, it turns out that this three-component-chain ($p2v$, SR , $b2a$) is extremely hard to train without supervision. Thus, we constrain the learning by employing another image-to-image translator, $a2b$, that translates from the input domain, A , to the output domain of our SR , B . To train these components ($p2v$, $a2b$, $b2a$), we introduce a **Reconstructive Adversarial Network (RAN)**. As can be seen in Section 5, training a RAN has strong similarities to training Generative Adversarial Networks (GANs) and especially Conditional Adversarial Networks. Like GANs, the RAN has a discriminator D , which plays an adversarial role. However, D in our case is trained to tell whether a pair of images from A and B comply (i.e., have similar content and respective styles), rather than to indicate whether the given image belongs to the target distribution or not.

These contributions constitute our novel architecture, consisting of the five elements depicted in Figure 1. The smooth renderer is explained in more detail in Section 3. The other components are simultaneously trained in a non-trivial manner through different data paths, as portrayed in Section 5. Once the prediction network $p2v$ (Section 4) has been trained, it is able to predict the 3D geometry of an object from one or more of its images. We show the results of this method in Section 6.

2. Related Work

Reconstructing 3D models from single or multiple images has been approached with different techniques. A number of recent works [1]–[6] have developed 3D reconstruction techniques based on supervision. In the following, we focus on methods that employ differentiable renderers.

The most common and efficient representation for 3D models is irregular polygonal meshes. Other representations, like voxel grids [12]–[15], [19]–[22], or points clouds [5], [23] are typically of lower resolution and do not scale well. Moreover, smoothly shading their discrete surfaces is difficult, and typically restricts to rendering only silhouettes [5], [12]–[14], [20], [23]. Working directly on meshes allows higher visual and computational quality while keeping memory footprint to a minimum.

Numerous works [7]–[11], [24]–[32] have presented differentiable renderers for 3D meshes. These renderers are differentiable with respect to lightning, geometry [7], [9]–[11], [24]–[28], material [26], [29]–[31], and/or texture [27], [29], [31]. As discussed in Section 3, however, these renderers are not differentiable on the entire domain (with respect to geometry, which is the relevant aspect when considering shape reconstruction). It is also possible to estimate a differentiable renderer with a Render-and-Compare-loss, which employs finite differences [33]. As can be expected, such an approach comes at the cost of computational effort and accuracy, compared to analytic gradients.

Rather than predicting, some works perform a mesh optimization process on a single 3D object [10], [24]–[28]. In these works, an initial mesh is optimized by iteratively changing its geometry, guided by back-propagated gradients. The main issue with such an approach is computational cost: this computationally expensive optimization process has to be repeated for every reconstruction. Prediction, on the other hand, is orders of magnitude faster [7]–[11].

For prediction, a proposed approach is to use auto-encoder-like networks to train a 3D mesh predicting encoder. If an object, and not just its silhouette, is differentially rendered, the auto-encoder-like network has an encoder-renderer structure predicting the 3D model in the latent space [7]–[9]. These encoder-render methods are typically restricted to reconstructing from images that match images produced by the employed differentiable renderer in appearance and style. Other works that render only the silhouette of an object [10]–[13] are only trained towards predicting proper ground truth silhouettes, while ignoring normals, and thus lighting.

Our work, in particular, the RAN, is closely related to Generative Adversarial Networks (GANs) [34], which allow generating new samples from a distribution, e.g., for generating voxel grids for a given class of objects [12], [14], [15], [19], [21]. These GANs can also be employed to

assist 3D reconstruction by supervising the appearance of reconstructions [12], [14], [15].

Finally, there are neural networks that are trained under supervision to render silhouettes from voxel grids [15], [35] or shaded images from a latent space [36].

3. C^∞ Smooth Renderer

In this section, we present our C^∞ Smooth Renderer that avoids any discontinuities at occlusions or dis-occlusions. Having this property, the renderer’s back-propagated gradients can be properly used to modify the 3D model. This is critical for integrating the renderer into a neural network. The typical discontinuity problem occurs during triangle rasterization, where the visibility of a triangle, due to occlusion or dis-occlusion, causes an abrupt change in the image. For example, if during the optimization process, the backside of a predicted object self-intersects its front, traditional differentiable renderers are not able to provide a reasonable gradient towards reversing such an erroneous self-intersection since they cannot differentiate with respect to occlusion. To overcome this problem, our approach offers a soft blending scheme, that is continuous even through such intersections.

As in the general rendering approach, first, we apply view transformations on all triangles to bring them from object

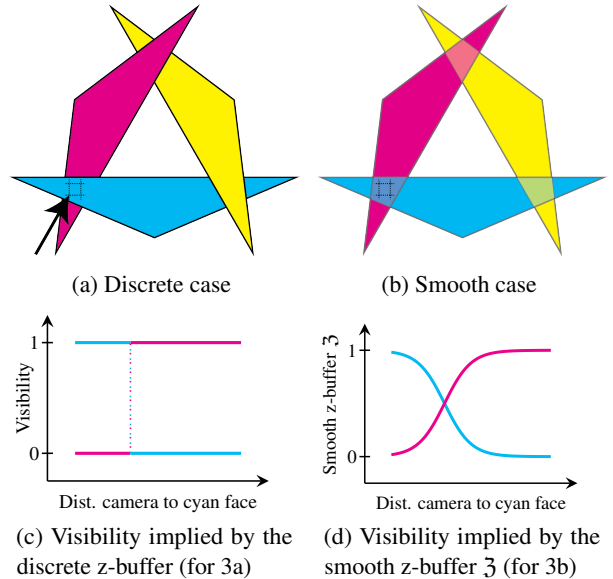


Figure 3: Visualization of the smooth depth buffer and occlusion: 3a shows three triangles rendered in a standard way, in 3b the same triangles are rendered smoothly. While in the discrete case a small change in depth can result in a sudden change of color (3c, our smooth depth-oriented rendering 3d) avoids that and therefore is differentiable everywhere.

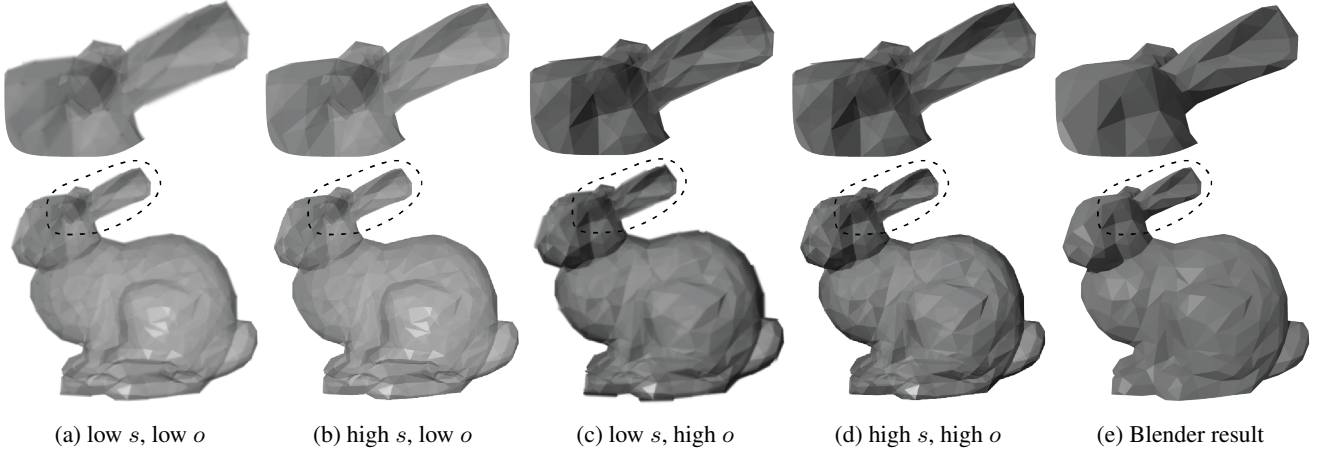


Figure 4: Stanford bunny rendered by the smooth renderer using different edge smoothnesses (s) and opacities (o): In 4a and 4b, the low opacity o causes, e.g., one of the ears to be still visible through the head of the bunny (for usage of o see section 3.1). In 4a and 4c, the low edge steepness causes smoother edges (for usage of s see section 3.2). On the right: The Stanford bunny rendered by Blender (e).

space into perspective projection space coordinates. This process is generally already fully differentiable.

Consecutively, one needs rasterization to correlate triangles to pixels. General rasterization consists of two steps, for each pixel one needs to collect all the triangles that cover that pixel, and then employ a z-buffer to determine which of them is visible in the pixel.

Instead of collecting all triangles that fit the xy-coordinates of a given pixel, we determine a probability value of whether a triangle fits a pixel for each triangle and pixel. This constitutes the visibility tensor V as shall be described in section 3.2.

Our key idea is to use a visibility test that enables reasoning beyond occlusion, using only smooth functions to avoid abrupt changes. Rather than taking a discrete decision of which triangle is the closest and thus visible, we softly blend their visibility, which goes along with an idea from stabilizing non-photorealistic rendering results [37]. By using a SoftMin-based function, we determine the closest and thus most visible face. But using the simple SoftMin of the z-positions in camera space would result in only the single closest triangle being most visible. Thus, we need to incorporate the visibility tensor V that tells us which triangles cover a given pixel. Instead, we weight the SoftMin with the visibility tensor V by introducing the weighted SoftMin ($\mathfrak{w}\text{SoftMin}$). Taking the $\mathfrak{w}\text{SoftMin}$ of the z-positions in camera space, constitutes smooth z-buffer as shall be described in greater detail in section 3.1.

This smooth z-buffer leads to our C^∞ Smooth Renderer, where the z-positions of triangles is differentiable with respect to occlusions. In previous differentiable renderers, only the xy-coordinates were locally differentiable with respect

to occlusion.

Let us assume to have three triangles (see Fig. 3a), where we want to examine the behavior of the bottom left pixel (marked with #) with respect to the z-position of the cyan face. During the process of optimizing the geometry, triangles might change their order with regard to the depth and abrupt color changes might appear. As shown in Figure 3c, the color value of the pixel (implied by the rasterization of the triangles) is constant except for one single point. At this point of intersection, the rasterization is discontinuous; at all other points, the derivative with respect to the z-position is 0. Employing the smooth rasterization and smooth z-buffer as in Figure 3d, the visibility of a pixel is never absolute, but rather a soft blend. Thus, it is differentiable, and optimizations can be solved with simple gradient descent.

Finally, we need to compute the color values of the triangles. For that, we use a lightning model composed of Blinn-Phong, diffuse, and ambient shading. We restrict the color to grayscale since we do not reconstruct the color in the RAN. Since the function of color is already differentiable we can directly use it.

Figure 4 shows a comparison between our smooth renderings and a Blender rendering of the Stanford bunny.

3.1. Smooth Z-buffer 3

Our rasterization is similar to the z-buffer algorithm, but instead of a displaying the single closet triangle and its z-distance in each pixel, we display a blend of triangles that project to the pixel.

We define the Smooth z-buffer \mathfrak{z} for pixel (p_x, p_y) ,

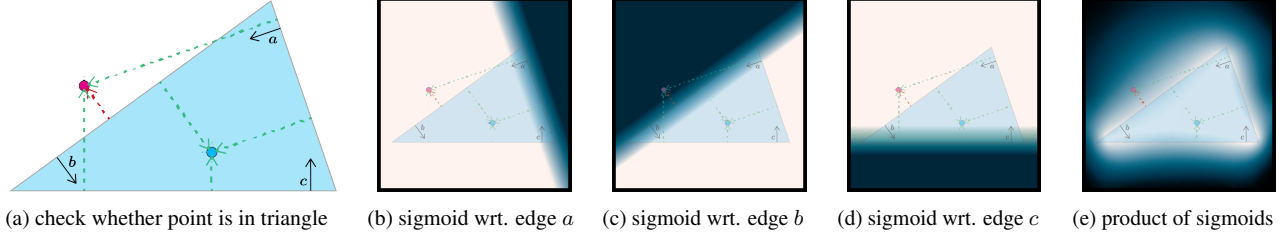


Figure 5: Visualization of the smooth rasterization. While the magenta point lies outside the triangle, the cyan point lies inside the triangle; this can be determined by measuring on which side of the edges a point lies. In subfigure 5b–5d it is smoothly determined which parts of the image lie inside and which parts lie outside the triangle with respect to the edges a – c . This is combined by multiplication (visibility tensor V) in subfigure 5e.

triangle T , and opacity o as follows:

$$\mathfrak{Z}(p_x, p_y, T) := \mathfrak{wSoftMin}(o \cdot \text{z-dist}(\text{camera}, T), \quad V(p_x, p_y, \cdot))$$

We define the weighted SoftMin (analogue to SoftMin/SoftMax) as: $\mathfrak{wSoftMin}(\mathbf{x}, w) := \mathfrak{wSoftMax}(-\mathbf{x}, w)$ where the weighted SoftMax is defined as:

$$\begin{aligned} \mathfrak{wSoftMax}_i(\mathbf{x}, w) &:= \frac{\exp(\mathbf{x}_i) \cdot w_i}{\sum_{i=0}^{\|w\|-1} \exp(\mathbf{x}_i) \cdot w_i} \\ &= \text{SoftMax}_i(\mathbf{x}_i + \log w_i) \end{aligned}$$

Thus, for a pixel, the closest triangle is represented with high visibility, while triangles further away have weaker visibility. The visibility tensor V , as shall be defined in Section 3.2, contains the extent to which a given triangle covers a given pixel. We use it as a weight for the $\mathfrak{wSoftMin}$, which allows considering only the relevant triangles in the SoftMin operator.

The opacity o is a hyper-parameter setting accelerating the strength of the SoftMin. See Figure 4 to see how it affects the results.

Similar to the painter’s algorithm [38], for performance reasons, we do not explicitly handle special cases of cyclic overlapping polygons that can cause the painter’s algorithm to fail. Nevertheless, our smooth renderer is not sensitive to these cases because when polygons are similarly distant from the camera, their opacity will also be very similar and thus not only the front polygon but also the rear one is visible.

3.2. Visibility tensor V

In the general rendering approach, the discrete choice, whether a triangle covers a pixel is just a trivial check. In the smooth approach, as shown in Figure 5, we determine the pixels that correspond to a triangle by checking for each pixel whether the directed distances from the pixel to each edge are

all positive. This yields the visibility tensor V for triangle $T = (e_1, e_2, e_3)$ with $e_i = (v_1, v_2)$ and $v_i = (v_{i,x}, v_{i,y})$, and steepness s as follows:

$$\begin{aligned} V(p_x, p_y, T) &:= \prod_{e=(v_1, v_2) \in T} \sigma \left(\begin{vmatrix} v_{x,2} - v_{x,1} & v_{x,1} - p_x \\ v_{y,2} - v_{y,1} & v_{y,1} - p_y \end{vmatrix} \cdot \frac{s}{m} \right) \\ &\text{with } m = \text{SoftMin}_{e \in T}(\|e\|) \end{aligned}$$

The sign of the directed distances to the three edges indicates on which side of the edge a pixel is. By applying a sigmoid function (σ) on that directed distances, we get a value close to 1 if the pixel lies inside and a value close to 0 if the pixel lies outside the triangle with respect to a given edge. By taking the product of the values for all three edges, the result ($\in [0, 1]$) smoothly indicates whether a pixel lies in or outside a triangle. Since this draws the triangles only from one direction, we add the same term with the negative directed distances to make the visibility tensor triangle orientation invariant:

$$\begin{aligned} V_{\text{orient.inv.}}(p_x, p_y, T) &= \sum_{a \in \{-1, 1\}} \prod_{e=(v_1, v_2) \in T} \sigma \left(a \begin{vmatrix} v_{x,2} - v_{x,1} & v_{x,1} - p_x \\ v_{y,2} - v_{y,1} & v_{y,1} - p_y \end{vmatrix} \frac{s}{m} \right) \end{aligned}$$

For Figure 5, the visibility tensor V looks as follows:

$$\begin{aligned} V(p_x/p_x, p_y/p_y, T) &\stackrel{\text{example}}{=} \left(\begin{array}{c} \text{Sigmoid curve} \\ \text{Distance } a \end{array} \right) \\ &\cdot \left(\begin{array}{c} \text{Sigmoid curve} \\ \text{Distance } b \end{array} \right) \cdot \left(\begin{array}{c} \text{Sigmoid curve} \\ \text{Distance } c \end{array} \right) \end{aligned}$$

The steepness s is a hyper-parameter setting the steepness of the sigmoid function. See Figure 4 to see how it affects the results.

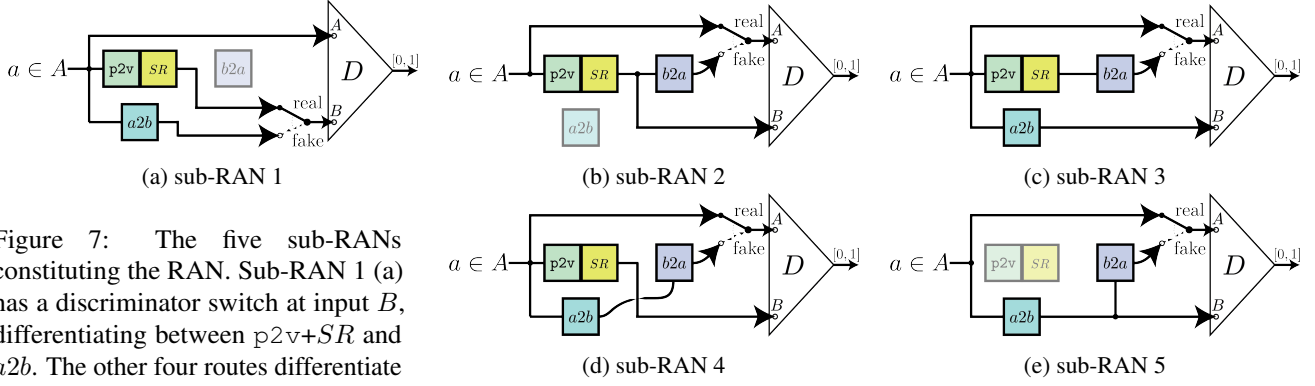


Figure 7: The five sub-RANs constituting the RAN. Sub-RAN 1 (a) has a discriminator switch at input B , differentiating between $p2v+SR$ and $a2b$. The other four routes differentiate between two images from space A , while the “real” input for the discriminator is always the input image. The “fake” input is the result of a round trip that either involves $p2v+SR$ and $b2a$ (b, c) or $a2b$ and $b2a$ (d, e). This round trip is required for a cycle-consistency loss that diminishes mode collapse. Meanwhile, the B input is the result of either $p2v+SR$ (b, d) or $a2b$ (c, e).

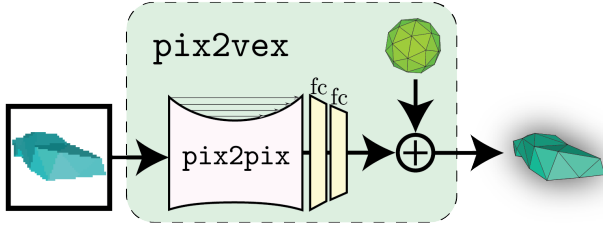


Figure 8: The reconstructor network’s $pix2vex$ architecture.

4. Reconstructor ($pix2vex$)

The reconstructor $pix2vex$ ($p2v$ in the figures) is the network that translates from images to a 3D model. The view directions of the input images are for most of our experiments fixed. The $pix2vex$ architecture is based on a $pix2pix$ convolutional and deconvolutional ResNet ([39]) network. The output of the $pix2pix$ is followed by two fully connected layers bringing it to a size of $3 \times \#vertices$. This is followed by a sigmoid layer and a linear transformation to bring the values into a range of $[-1, 1]$. These values are considered as vectors and then added to the vertices of the base model, a uniform sphere with a predefined topology. In our experiments, we have found that starting the training from an object, such as the sphere, and predicting offsets from it, evolves in a better and smoother way towards convergence, when compared to predicting absolute coordinates.

To reconstruct models that contain symmetry we can optionally use a more canonical way of displacing vertices from an initial model to the prediction. That is, we split our model into four equal quarters w.r.t. a top-down view. Firstly, we predict a quarter of the model by applying shifts to the base model of that quarter. Then we mirror the predicted quarter to another quarter and predict the shifts to displace

the mirrored quarter. We do this until all four quarters are predicted. This implies the gradients that would usually only move one side to imply a movement on all sides.

In addition, we also predict uniform translation and scaling values, which assist in reducing the overall offset values magnitude, and thus improve system stability.

Lastly, we also apply regularization on the 3D mesh, which guide the prediction towards more reasonably shaped reconstructed meshes. These regularizations consider angles between normals, edge lengths, and curvature, as shall be described in more detail in Appendix A.1.

5. RAN

Our Reconstructive Adversarial Network (RAN) is a framework to train the reconstructor ($pix2vex$) without 3D supervision, i.e., without the need for the actual 3D models corresponding to the input images during training. This means that we need another way to evaluate the predictions. In other words, we let the RAN learn a supervision by itself. The challenge here is the following causality dilemma: To train the reconstruction, we need to compare the smoothly rendered images of the predicted shape to the input, which requires style transfer. On the other hand, in order to train the style translation, we need to know what a properly smoothly rendered image (corresponding to the input image) looks like. A typical approach for solving such causality dilemmas is to solve the two components evolutionarily by iteratively applying various influences towards a common solution.

The key idea is to train an adversarial discriminator D to discriminate between the different ways to obtain pairs of images from A (identity, $p2v-SR-b2a$, $a2b-b2a$) and B ($p2v-SR$, $a2b$). This allows the three components $p2v$, $a2b$ and $b2a$ to be trained to fool D . In designing such a strategy, we exploited the following insights:

- Since $pix2pix$ networks are lazy and their capabilities are restricted, the discriminator can be implicitly trained

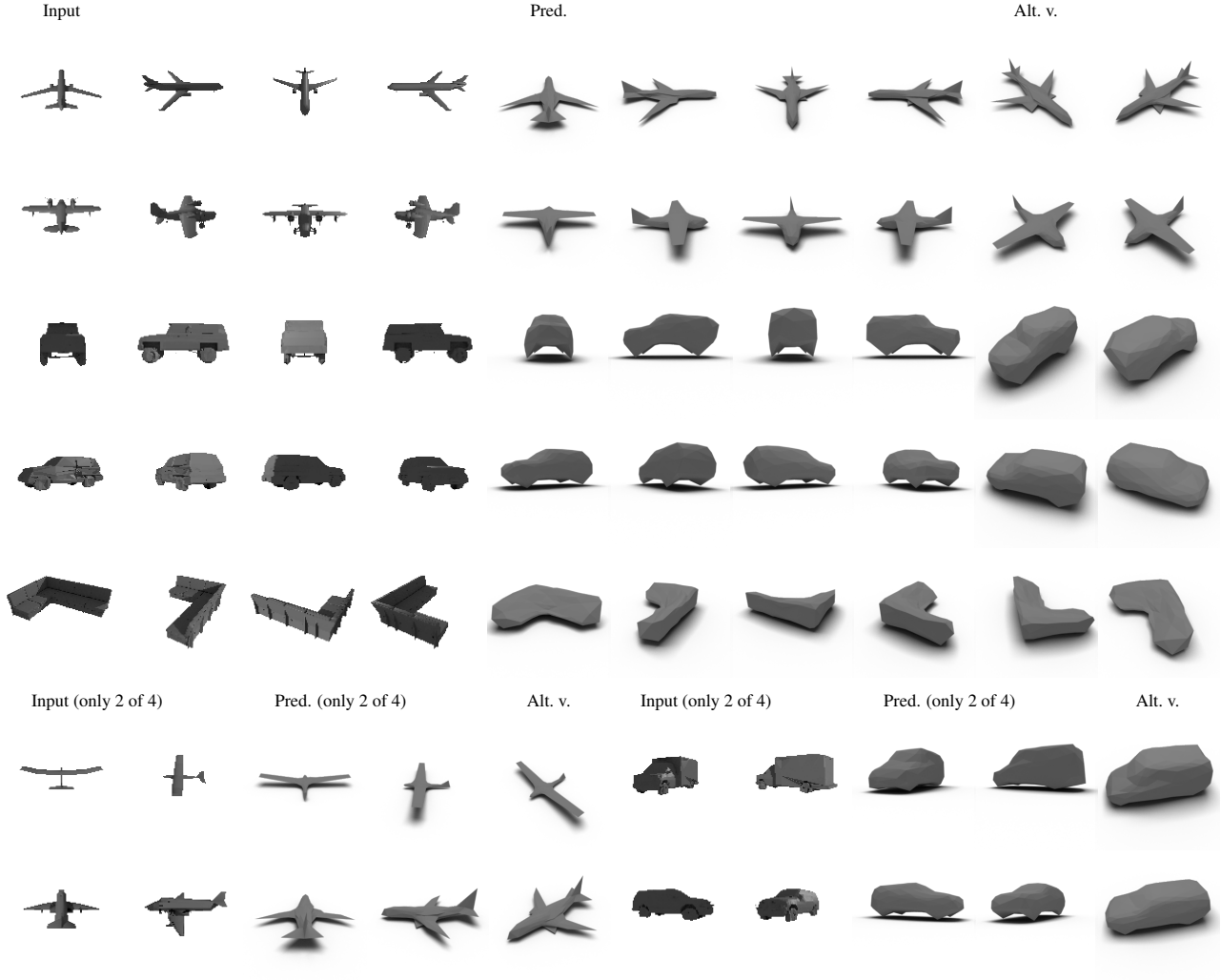


Figure 9: Results for the four-view reconstruction of the ShapeNet [40] classes *airplane*, *car*, and *sofa*. On the left is the input, in the middle the prediction from the same angles, and on the right are the predictions from alternative viewpoints.

in a way that the content between pairs of images (A and B) will be similar. The rationale behind this is the following: for the pix2pix to hold the cycle-consistency of p2v-SR-b2a , it is much easier for the image translator to only do a style-transfer from a content-wise similar image than to reconstruct the input from a smooth rendering of an entirely different object.

- By smoothly rendering random guessed 3D models, we train the discriminator to know what a general smoothly rendered image should look like. After doing so, the discriminator can be used to train $a2b$ to output images from B .

Training a conventional GAN is a relatively straightforward task, since only a single binary decision (real vs. fake) is to be done. Training the RAN, as shown in Fig. 1, is much more convoluted, since instead of only

one binary decision, two decisions have to be made: one between three choices (A -input real vs. fake generated by p2v-SR-b2a vs. $a2b-b2a$) and one between two choices (B -input only fake generated by p2v-SR vs. $a2b$). These paths represent all possibilities to obtain an image of A respectively B —i.e., the discriminator has to differentiate between all possible ways to generate its input; fooling the discriminator leads to a common solution for all these paths.

Since it is easier to train a binary discriminator, our solution is to break the RAN into five sub-RANs, where each of which has a single binary decision to make (real vs. fake), as depicted in Figure 7. These sub-RANs are alternately trained like conventional GANs; that is, training the discriminator to differentiate between the “real” and “fake” input and training the other modules to fool the discriminator. If there are two modules to be trained at once, the training is split into two steps: the module next to the

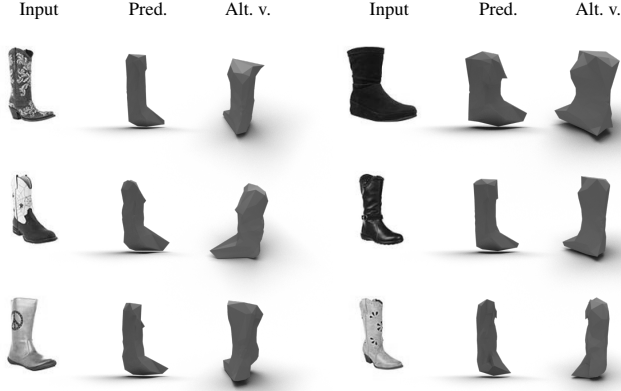


Figure 10: Single-view reconstruction results from the UT Zappos50K dataset. Although the shoes have strong textures, the shoes are adequately reconstructed.

discriminator is trained first and the earlier one second. This helps in avoiding mode collapse. Since the relevance of these sub-RANs differs, their influence is weighted. For example, training a path with the `pix2vex` module (sub-RAN (a) in Figure 7) carries more weight than training the cycle of the two image translators (sub-RAN (e)). For the discriminator D , we use the binary cross-entropy loss. For training, an L^1 loss between any two images of the same image space is applied. Losses shall be described in detail in Appendix A.1.

This constitutes the RAN as an unsupervised way to find an appropriate internal representation which requires the `pix2pix` networks to perform a minimum of content-wise changes.

6. Results

We evaluate our reconstruction results on synthetic as well as camera-captured images. While using synthetic images allow highly controlled experiments, training and evaluating on camera-captured images shows that our approach is also applicable in real-world scenarios.

For creating synthetic images, we used the ShapeNet dataset [40]. ShapeNet is a dataset of categorized 3D meshes that has also been used for many other 3D reconstruction tasks. We rendered the 3D meshes using Blender with a resolution of typically 128×128 and from multiple directions. For that, we used lighting hyperparameters different from the lighting hyperparameters that we used in the *SR* of the RAN. In the general case we used sets of images from four ($\Delta_{\text{azimuth}} = 90 \text{ deg}$) azimuths for our training. The results for this setting are shown in Fig. 9. In addition, we conducted studies on modified settings as presented and described in Fig. 11.

For training on camera-captured images, we used

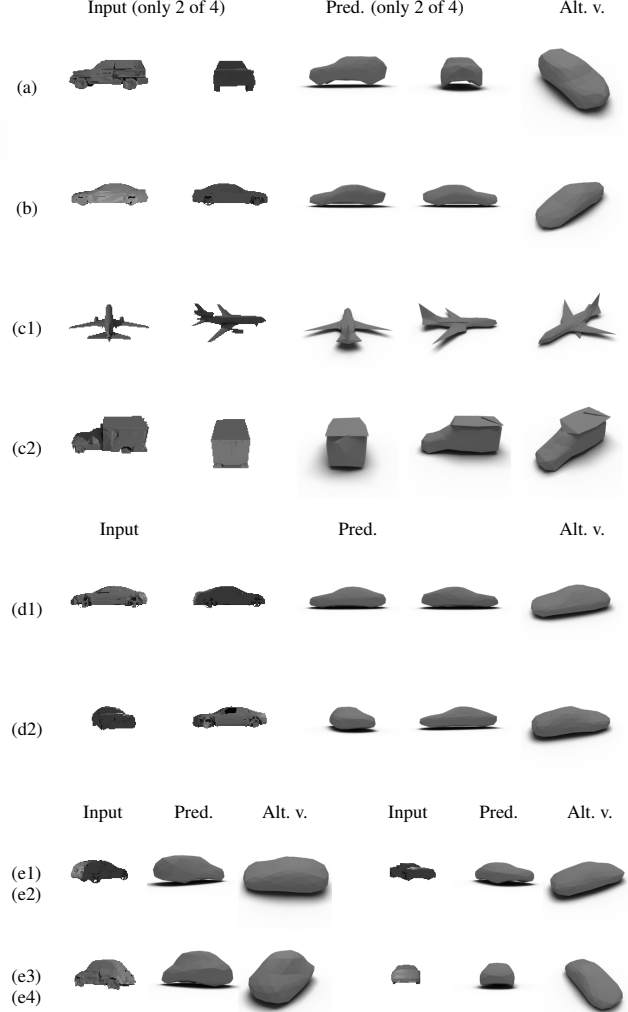


Figure 11: Experiments showing the robustness of our approach. In (a–c), we performed four-view trainings with the following modifications to the training data: In (a), we randomized the azimuth of the images with a standard deviation of 5° . In (b), we randomly assigned the position of the light source for each set of images. In (c1–c2), we trained on the *car* and *airplane* classes simultaneously. In (d–e), we randomized, but supervised, the difference between azimuths for the four images. I.e., if multiple images have the same azimuth, the input data is effectively three or fewer images. In (d1–d2), we predicted the images from only two input images; in (e1–e4), we show single-view reconstructions.

same-directional single-view images of shoes [41]. Since these images are only single-view images, even typically from more or less the same direction, we use a mirrored version of the image and pretend that it is the view from the other side. We employed this small trick

since many objects such as shoes are commonly roughly symmetric. Moreover, the back of the shoe could not be reconstructed without even having any training sample from the back side. Since this problem is highly ill-posed, our results could still be improved—nevertheless, they are the first of their kind. Fully unsupervised consistently-same-direction-single-view 3D mesh reconstruction results for training on camera-captured images are presented in Fig. 10.

7. Discussion and Conclusion

In this work, we have demonstrated a robust way to reconstruct 3D geometry from only 2D data, eliminating the need for ground truth 3D models, or prior knowledge regarding materials and lighting conditions. In addition, we have demonstrated how a globally differentiable renderer is crucial to the learning process—even if designing one induces differences in the appearance of the produced renderings. We alleviate this difference through the use of image domain translation. The success of the reconstruction is driven by a restriction of the information flow and by the laziness of `pix2pix` networks, which easily perform image-style exchanges but struggle in changing the content of an image—a property that we exploit. Thus, our approach is not informed by data but instead by an understanding of the real world.

In addition, we believe that our RAN architecture is suitable to more than just its current application of 3D reconstruction, but rather to a variety of inverse problems. To do so, one could replace the smooth renderer with another smooth forward simulator to reconstruct the inverse of the respective algorithm without supervision. In such a case, we would also distinguish between spaces A and B since the output of the smooth simulator is generally different from the output of its discrete counterpart. Depending on the problem, it can be useful to shortcut the smooth algorithm to let the discriminator also consider the reconstructed space.

The source code of our work will be publicly available.

This novel architecture potentially leads to many interesting lines of future investigation. The immediate direction would be training the reconstruction from single images. The problem of training 3D reconstructions using a single view approach is, of course, the fact that the occluded side of the model is unknown. We have overcome this issue by initially using training data from multiple viewpoints to familiarize the network with objects of a certain class, and then gradually switching to training the system to infer shapes using only a single image. Another approach would be to use a differentiable renderer to create training images by supervising 3D shapes, materials and light settings. This approach must be handled with care—while this is possible for synthetic settings, where the images can be rendered using an equivalent renderer, this is not possible when

working with camera-captured images.

In addition, we believe the RAN could be adapted to camera-captured single-view image 3D reconstructions, given the right training dataset.

Another interesting path would be to allow decoding information like textures in the internal smooth image space. This could be done through adding (non-realistic) colors to the smooth renderer which would increase the representative power of the mentioned internal image space. It would also be interesting to further extend the developed renderer to support also global illumination, which would enable the reconstructions of whole scenes.

Finally, we hope to inspire the research community to explore the full power of our smooth forward simulator and RAN architecture. We believe that it can be used for many other research objectives, such as the inverse-problem of iterated function systems or an unsupervised speech-to-text translation.

References

- [1] H. Fan, H. Su, and L. Guibas, “A Point Set Generation Network for 3D Object Reconstruction from a Single Image,” Dec. 2016. [Online]. Available: <http://arxiv.org/abs/1612.00603>.
- [2] P. Achlioptas, O. Diamanti, I. Mitliagkas, and L. Guibas, “Learning Representations and Generative Models for 3D Point Clouds,” Jul. 2017. [Online]. Available: <http://arxiv.org/abs/1707.02392>.
- [3] C. B. Choy, D. Xu, J. Y. Gwak, K. Chen, and S. Savarese, “3D-R2N2: A unified approach for single and multi-view 3D object reconstruction,” *Lecture Notes in Computer Science (including subseries Lecture Notes in Artificial Intelligence and Lecture Notes in Bioinformatics)*, vol. 9912 LNCS, no. 3, pp. 628–644, 2016, ISSN: 16113349. DOI: 10.1007/978-3-319-46484-8{_}38. [Online]. Available: <https://arxiv.org/abs/1604.00449>.
- [4] N. Wang, Y. Zhang, Z. Li, Y. Fu, W. Liu, and Y.-G. Jiang, “Pixel2Mesh: Generating 3D Mesh Models from Single RGB Images,” Apr. 2018. [Online]. Available: <http://arxiv.org/abs/1804.01654>.
- [5] L. Jiang, S. Shi, X. Qi, and J. Jia, “GAL: Geometric adversarial loss for single-view 3D-object reconstruction,” *Lecture Notes in Computer Science (including subseries Lecture Notes in Artificial Intelligence and Lecture Notes in Bioinformatics)*, vol. 11212 LNCS, pp. 820–834, 2018, ISSN: 16113349. DOI: 10.1007/978-3-030-01237-3{_}49.
- [6] A. Kurenkov, J. Ji, A. Garg, V. Mehta, J. Gwak, C. Choy, and S. Savarese, “DeformNet: Free-form deformation network for 3D shape reconstruction from a single image,” *Proceedings - 2018 IEEE Winter Conference on Applications of Computer Vision, WACV 2018*, vol. 2018-Janua, no. i, pp. 858–866, 2018. DOI: 10.1109/WACV.2018.00099.

- [7] C. Che, F. Luan, S. Zhao, K. Bala, and I. Gkioulekas, "Inverse Transport Networks," Sep. 2018. [Online]. Available: <http://arxiv.org/abs/1809.10820>.
- [8] P. Henderson and V. Ferrari, "Learning to Generate and Reconstruct 3D Meshes with only 2D Supervision," Jul. 2018. [Online]. Available: <https://arxiv.org/abs/1807.09259>.
- [9] E. Richardson, M. Sela, R. Or-El, and R. Kimmel, "Learning detailed face reconstruction from a single image," *Proceedings - 30th IEEE Conference on Computer Vision and Pattern Recognition, CVPR 2017*, vol. 2017-Janua, pp. 5553–5562, 2017, ISSN: 1063-6919. DOI: 10.1109/CVPR.2017.589.
- [10] H. Kato, Y. Ushiku, and T. Harada, "Neural 3D Mesh Renderer," Nov. 2017, ISSN: 0157244X. DOI: 10.1109/CVPR.2018.00411. [Online]. Available: <http://arxiv.org/abs/1711.07566>.
- [11] S. Liu, W. Chen, T. Li, and H. Li, "Soft Rasterizer: Differentiable Rendering for Unsupervised Single-View Mesh Reconstruction," Jan. 2019. [Online]. Available: <https://arxiv.org/abs/1901.05567>.
- [12] M. Gadelha, S. Maji, and R. Wang, "3D Shape Induction from 2D Views of Multiple Objects," Dec. 2016. [Online]. Available: <http://arxiv.org/abs/1612.05872>.
- [13] X. Yan, J. Yang, E. Yumer, Y. Guo, and H. Lee, "Perspective Transformer Nets: Learning Single-View 3D Object Reconstruction without 3D Supervision," vol. d, no. Nips, pp. 1–15, 2016, ISSN: 10495258. [Online]. Available: <http://arxiv.org/abs/1612.00814>.
- [14] J. Gwak, C. B. Choy, A. Garg, M. Chandraker, and S. Savarese, "Weakly supervised 3D Reconstruction with Adversarial Constraint," May 2017. [Online]. Available: <https://arxiv.org/abs/1705.10904>.
- [15] D. J. Rezende, S. M. A. Eslami, S. Mohamed, P. Battaglia, M. Jaderberg, and N. Heess, "Unsupervised Learning of 3D Structure from Images," Jul. 2016. [Online]. Available: <http://arxiv.org/abs/1607.00662>.
- [16] A. Kar, S. Tulsiani, J. Carreira, and J. Malik, "Category-specific object reconstruction from a single image," *Proceedings of the IEEE Computer Society Conference on Computer Vision and Pattern Recognition*, vol. 07-12-June, pp. 1966–1974, 2015, ISSN: 10636919. DOI: 10.1109/CVPR.2015.7298807.
- [17] S. Vicente, J. Carreira, L. Agapito, and J. Batista, "Reconstructing PASCAL VOC," in *Proceedings of the 2014 IEEE Conference on Computer Vision and Pattern Recognition*, ser. CVPR '14, Washington, DC, USA: IEEE Computer Society, 2014, pp. 41–48, ISBN: 978-1-4799-5118-5. DOI: 10.1109/CVPR.2014.13. [Online]. Available: <https://doi.org/10.1109/CVPR.2014.13>.
- [18] A. Kanazawa, S. Tulsiani, A. A. Efros, and J. Malik, "Learning Category-Specific Mesh Reconstruction from Image Collections," Mar. 2018. [Online]. Available: <https://arxiv.org/abs/1803.07549>.
- [19] P. Henzler, N. Mitra, and T. Ritschel, "Escaping Plato's Cave using Adversarial Training: 3D Shape From Unstructured 2D Image Collections," 2018. [Online]. Available: <http://arxiv.org/abs/1811.11606>.
- [20] S. Tulsiani, T. Zhou, A. A. Efros, and J. Malik, "Multi-view Supervision for Single-view Reconstruction via Differentiable Ray Consistency," Apr. 2017. [Online]. Available: <http://arxiv.org/abs/1704.06254>.
- [21] J.-Y. Zhu, Z. Zhang, C. Zhang, J. Wu, A. Torralba, J. B. Tenenbaum, and W. T. Freeman, "Visual Object Networks: Image Generation with Disentangled 3D Representation," Dec. 2018. [Online]. Available: <http://arxiv.org/abs/1812.02725>.
- [22] J. Wu, Y. Wang, T. Xue, X. Sun, W. T. Freeman, and J. B. Tenenbaum, "MarrNet: 3D Shape Reconstruction via 2.5D Sketches," Nov. 2017. [Online]. Available: <https://arxiv.org/abs/1711.03129>.
- [23] N. K. L., P. Mandikal, M. Agarwal, and R. V. Babu, "CAPNet: Continuous Approximation Projection For 3D Point Cloud Reconstruction Using 2D Supervision," Nov. 2018. [Online]. Available: <http://arxiv.org/abs/1811.11731>.
- [24] M. M. Loper and M. J. Black, "OpenDR: An approximate differentiable renderer," *Lecture Notes in Computer Science (including subseries Lecture Notes in Artificial Intelligence and Lecture Notes in Bioinformatics)*, vol. 8695 LNCS, no. PART 7, pp. 154–169, 2014, ISSN: 16113349. DOI: 10.1007/978-3-319-10584-0{_}11.
- [25] T.-M. Li, M. Aittala, F. Durand, and J. Lehtinen, "Differentiable Monte Carlo ray tracing through edge sampling," *SIGGRAPH Asia 2018 Technical Papers on - SIGGRAPH Asia '18*, vol. 37, no. 6, pp. 1–11, 2018, ISSN: 07300301. DOI: 10.1145/3272127.3275109. [Online]. Available: <http://dl.acm.org/citation.cfm?doid=3272127.3275109>.
- [26] S. P. Bangaru, *Towards Shape Reconstruction through Differentiable Rendering*, MSc Thesis, 2019.
- [27] H.-T. D. Liu, M. Tao, C.-L. Li, D. Nowrouzezahrai, and A. Jacobson, "Adversarial Geometry and Lighting using a Differentiable Renderer," 2018. DOI: arXiv:1808.02651v1. [Online]. Available: <http://arxiv.org/abs/1808.02651>.
- [28] A. Delaunoy, E. Prados, A. Delaunoy, E. Prados, and G. Flows, "Gradient Flows for Optimizing Triangular Mesh-based Surfaces : Applications to 3D Reconstruction Problems dealing with Visibility To cite this version : HAL Id : inria-00546105 Gradient Flows for Optimizing Triangular Mesh-based Surfaces : Applications to," 2011.
- [29] R. Ramamoorthi and P. Hanrahan, "A signal-processing framework for inverse rendering," *Proceedings of the 28th annual conference on Computer graphics and interactive techniques - SIGGRAPH '01*, pp. 117–128, 2001, ISSN: 0097-8930. DOI: 10.1145/383259.383271. [Online]. Available: <http://portal.acm.org/citation.cfm?doid=383259.383271>.

- [30] A. Meka, M. Maximov, M. Zollhoefer, A. Chatterjee, H.-P. Seidel, C. Richardt, and C. Theobalt, "LIME: Live Intrinsic Material Estimation," 2018, ISSN: 1522-8517. DOI: 10.1109/CVPR.2018.00661. [Online]. Available: <http://arxiv.org/abs/1801.01075>.
- [31] A. Athalye, L. Engstrom, A. Ilyas, and K. Kwok, "Synthesizing Robust Adversarial Examples," Jul. 2017. [Online]. Available: <http://arxiv.org/abs/1707.07397>.
- [32] A. Palazzi, L. Bergamini, S. Calderara, and R. Cucchiara, "End-to-End 6-DoF Object Pose Estimation Through Differentiable Rasterization," pp. 702–715, 2019. DOI: 10.1007/978-3-030-11015-4{_}53.
- [33] A. Kundu, Y. Li, and J. M. Rehg, "3D-RCNN: Instance-level 3D Object Reconstruction via Render-and-Compare," *Cvpr*, 2018. DOI: 10.1109/CVPR.2018.00375. [Online]. Available: http://openaccess.thecvf.com/content_cvpr_2018/papers/Kundu_3D-RCNN_Instance-Level_3D_CVPR_2018_paper.pdf.
- [34] I. J. Goodfellow, J. Pouget-Abadie, M. Mirza, B. Xu, D. Warde-Farley, S. Ozair, A. Courville, and Y. Bengio, "Generative Adversarial Networks," Jun. 2014. [Online]. Available: <https://arxiv.org/abs/1406.2661>.
- [35] T. Nguyen-Phuoc, C. Li, S. Balaban, and Y.-L. Yang, "RenderNet: A deep convolutional network for differentiable rendering from 3D shapes," Jun. 2018. [Online]. Available: <http://arxiv.org/abs/1806.06575>.
- [36] S. M. Eslami, D. Jimenez Rezende, F. Besse, F. Viola, A. S. Morcos, M. Garnelo, A. Ruderman, A. A. Rusu, I. Danihelka, K. Gregor, D. P. Reichert, L. Buesing, T. Weber, O. Vinyals, D. Rosenbaum, N. Rabinowitz, H. King, C. Hillier, M. Botvinick, D. Wierstra, K. Kavukcuoglu, and D. Hassabis, "Neural scene representation and rendering," *Science (New York, N.Y.)*, vol. 360, no. 6394, pp. 1204–1210, 2018, ISSN: 10959203. DOI: 10.1126/science.aar6170.
- [37] T. Luft, O. Deussen, T. Luft, and O. Deussen, "Real-time Watercolor Illustrations of Plants Using a Blurred Depth Test," *Proceedings of the 4th International Symposium on Non-photorealistic Animation and Rendering*, vol. 21, no. 2006, pp. 159–165, 2006. DOI: 10.1145/1124728.1124732.
- [38] M. de Berg, *Ray Shooting, Depth Orders and Hidden Surface Removal*, ser. Lecture Notes in Computer Science. Springer, 1993, ISBN: 9783540570202. [Online]. Available: https://books.google.co.il/books?id=b1INPTC3w_QC.
- [39] K. He, X. Zhang, S. Ren, and J. Sun, "Deep Residual Learning for Image Recognition," Dec. 2015. [Online]. Available: <https://arxiv.org/abs/1512.03385>.
- [40] A. X. Chang, T. Funkhouser, L. Guibas, P. Hanrahan, Q. Huang, Z. Li, S. Savarese, M. Savva, S. Song, H. Su, J. Xiao, L. Yi, and F. Yu, "ShapeNet: An Information-Rich 3D Model Repository," Dec. 2015. [Online]. Available: <https://arxiv.org/abs/1512.03012>.
- [41] A. Yu and K. Grauman, "Fine-Grained Visual Comparisons with Local Learning," in *Computer Vision and Pattern Recognition (CVPR)*, Jun. 2014.
- [42] D. P. Kingma and J. Ba, "Adam: {A} Method for Stochastic Optimization," *CoRR*, vol. abs/1412.6, 2014. [Online]. Available: <http://arxiv.org/abs/1412.6980>.

Appendices

A. Implementation details

A.1. Losses

Our optimization of p2v , $a2b$, $b2a$, and D involves adversarial losses, cycle-consistency losses, and mesh regularization losses. Specifically, we solve the following optimization:

$$\min_{\text{p2v}} \min_{a2b} \min_{b2a} \max_D \mathcal{L}$$

or in greater detail

$$\min_{\text{p2v}} \min_{a2b} \min_{b2a} \max_D \sum_{i=1}^5 (\alpha_i \cdot \mathcal{L}_i) + \mathcal{L}_{\text{reg}}.$$

where α_i is a weight in $[0, 1]$, \mathcal{L} , \mathcal{L}_i , and \mathcal{L}_{reg} shall be defined below.

We define $b', b'' \in B$ and $a', a'' \in A$ in dependency of $a \in A$ according to Fig. 1 as

$$\begin{aligned} b' &= a2b(a) \\ b'' &= SR \circ \text{p2v}(a) \\ a' &= b2a(b') \\ a'' &= b2a(b'') \end{aligned}$$

With that, our losses are

$$\begin{aligned} \mathcal{L}_1 &= \mathbb{E}_{a \sim A} [\log D(a, b'')] + \mathbb{E}_{a \sim A} [\log(1 - D(a, b'))] \\ &\quad + \mathbb{E}_{a \sim A} [\|b'' - b'\|_1] \\ \mathcal{L}_2 &= \mathbb{E}_{a \sim A} [\log D(a, b'')] + \mathbb{E}_{a \sim A} [\log(1 - D(a'', b''))] \\ &\quad + \mathbb{E}_{a \sim A} [\|a'' - a\|_1] \\ \mathcal{L}_3 &= \mathbb{E}_{a \sim A} [\log D(a, b')] + \mathbb{E}_{a \sim A} [\log(1 - D(a'', b'))] \\ &\quad + \mathbb{E}_{a \sim A} [\|a' - a\|_1] + \mathbb{E}_{a \sim A} [\|b'' - b'\|_1] \\ \mathcal{L}_4 &= \mathbb{E}_{a \sim A} [\log D(a, b'')] + \mathbb{E}_{a \sim A} [\log(1 - D(a', b''))] \\ &\quad + \mathbb{E}_{a \sim A} [\|a' - a\|_1] + \mathbb{E}_{a \sim A} [\|b'' - b'\|_1] \\ \mathcal{L}_5 &= \mathbb{E}_{a \sim A} [\log D(a, b')] + \mathbb{E}_{a \sim A} [\log(1 - D(a', b'))] \\ &\quad + \mathbb{E}_{a \sim A} [\|a' - a\|_1]. \end{aligned}$$

This results in our combined loss of (without weights)

$$\begin{aligned} \mathcal{L} &= \mathbb{E}_{a \sim A} [\log D(a, b'')] \\ &\quad + \mathbb{E}_{a \sim A} [\log D(a, b'')] \\ &\quad + \mathbb{E}_{a \sim A} [\log(1 - D(a, b'))] \\ &\quad + \mathbb{E}_{a \sim A} [\log(1 - D(a', b'))] \\ &\quad + \mathbb{E}_{a \sim A} [\log(1 - D(a', b''))] \\ &\quad + \mathbb{E}_{a \sim A} [\log(1 - D(a'', b''))] \\ &\quad + \mathbb{E}_{a \sim A} [\|b'' - b'\|_1] \\ &\quad + \mathbb{E}_{a \sim A} [\|a' - a\|_1] \\ &\quad + \mathbb{E}_{a \sim A} [\|a'' - a\|_1] \\ &\quad + \mathcal{L}_{\text{reg}}. \end{aligned}$$

\mathcal{L}_{reg} are the regularization losses on the reconstructed meshes. These regularizations are presented with descending relevance:

The angle of normals of adjacent faces should be as similar as possible (loss uses the L^2 norm).

The lengths of edges should be as similar as possible (loss uses the L^1 norm).

The distance to the mean vertex of adjacent vertices should be as small as possible to imply a regular mesh and also reduce the curvature of the mesh (loss uses the L^1 norm).

A.1.1 Training procedure

We alternately train the different sections of our network in the following order:

1. The discriminator D
2. The translation from B to A ($b2a$)
3. The components that perform a translation from A to B ($\text{p2v} + \text{SR}$, $a2b$)

For each of these sections, we separately train the five losses \mathcal{L}_i . For that, we used the Adam optimizer [42] and started the training with a learning rate of 10^{-6} .

A.2. Network Architectures

Here, we describe the topologies of the components p2v , $a2b$, $b2a$, and D . In our experiments we typically used an image resolution of $n \times n = 128 \times 128$ and a number of vertices $v = 162$ —we will base the following details on that assumption.

Let Ck denote a Convolution–LeakyReLU layer with k filters of size 4×4 and a stride of 2. Let the negative slope of the LeakyReLU be 0.2. From the fifth convolutional layer on, we apply a 50% dropout.

The **pix2pix** network is a symmetric residual network with the following blocks defining the first half: C64-C128-C256-C512-C512-C512-C512

pix2vex is based on the **pix2pix** network. It is followed by two fully connected layers ($n^2 \rightarrow \left\lfloor \frac{n^2+3 \cdot v}{2} \right\rfloor$ and $\left\lfloor \frac{n^2+3 \cdot v}{2} \right\rfloor \rightarrow 3 \cdot v$) and the sigmoid function. The remainder of the **pix2vex** architecture is explained in Section 4 in greater detail.

a2b and **b2a** are **pix2pix** networks with the first two or more residual layers. This is followed by the sigmoid function.

The **discriminator D** is defined as C64-C128-C256-C512-C1 followed by the sigmoid function.

A.3. Stabilization of the smooth z-buffer

A problem of the in Section 3.1 described smooth z-buffer is that pixels that are not covered by any triangle can appear as if they had visible triangles. That's because, if all weights are very low, even weights close to zero can cause a high value in the weighted SoftMin. To stabilize this, we add two triangles covering the background and reduce the visibility value with increasing distance from triangles.